Adaptive strategies for recognition, noise filtering, control, synchronization and targeting of chaos

F. T. Arecchi
Instituto Nazionale di Ottica, I-50125 Firenze, Italy
and Department of Physics, University of Firenze, I-50125 Firenze, Italy

S. Boccaletti
Instituto Nazionale di Ottica, I-50125 Firenze, Italy
and Institut Non Lineaire de Nice, Sophia Antipolis, France

(Received 11 April 1997; accepted for publication 14 July 1997)

Combining knowledge of the local variation rates with some information on the long time trends of a dynamical system, we introduce an adaptive recognition technique consisting in a sequence of variable resolution observation intervals at which the geometrical positions are sampled. The sampling times are chosen so that the sequence of observed points forms a regularized set, in the sense that the separation of adjacent points is almost uniform. We show how this adaptive technique is able to recognize the unstable periodic orbits embedded within a chaotic attractor and stabilize anyone of them even in the presence of noise, through small additive corrections to the dynamics. These techniques have been applied to the synchronization of three chaotic systems, assuring secure communication between a message sender and a message receiver; furthermore they provide robust solutions to the problems of targeting of chaos and of filtering the noise out of an experimental chaotic data set. Implementation of adaptive methods to chaotic Lorenz, three and four dimensional Roessler models and Mackey-Glass delayed system are reported. © *1997 American Institute of Physics.* [S1054-1500(97)00604-6]

We present here a new adaptive recognition method that, when applied to a chaotic time series, extracts some key features of the temporal behavior with a minimal amount of computational effort. Examples of information that can be obtained include the maximum Lyapunov exponent, an indicator of determinism versus stochasticity, and the positions of the unstable periodic orbits contained in the chaotic attractor. Adaptive recognition does not aim at reconstructing the geometry of the motion, but it is limited to a one-dimensional string of data, namely, a sequence of observation time intervals selected by a suitable variational technique. We show how this method is effective in recovering the deterministic part of a noisy chaotic signal, in controlling chaos by stabilizing one of the unstable periodic orbits, in synchronizing two chaotic systems ruled by the same dynamical equations, and in targeting chaos, that is, steering the orbit toward a specific point within a conveniently short time.

I. INTRODUCTION

Two different strategies are used to inspect a (possibly continuous) dynamical system: the standard one whereby one fixes a sequence of regularly spaced observation times and plots the corresponding positions in some coordinate space. The geometry of such a time series of data discriminates on whether a signal is regular, chaotic, or random. An alternative strategy consists in fixing a given resolution in the coordinate space and registering only the subset of the whole signal consisting of those points such that the separation of two successive ones is within that resolution. The corresponding geometric set is an almost regular one, but the sequence of stroboscopic observation times is now erratic when the considered dynamics is irregular. At variance with the geometry of a time series, which yields a set of points embedded in a N dimensional space, the stroboscopic times provide a one dimensional string of data.

This implies that for such a strategy the indicators of chaotic motion, based on the mutual distances of points in state space[1] are not manageable. On the contrary, all those indicators relying on the time information, as e.g. the maximum Lyapunov exponent, the location and stability of the unstable periodic orbits of a chaotic attractor and the signal to noise ratio within a frequency range, are easily accessible to our method with a computation time which increases linearly rather than exponentially with the number of dimensions. As a result, application of these time indicators has become more convenient as we will show.

In this report we will review the results of recent studies, whereby this adaptive strategy introduced for recognition (Sec. II) and noise filtering (Sec. III) is applied to control (Sec. IV), synchronization (Sec. V) and targeting (Sec. VI). In all cases we provide critical comparison with alternative approaches, discussing merits and limitations of our method.

II. CHAOS RECOGNITION

The standard description of a dynamical system is done by selecting a uniform sequence of observation times (i.e., separated by a constant time interval) and plotting the evolution of the corresponding positions in some coordinate

space. Based upon the geometry of the time series, one extracts suitable indicators to classify a signal as regular, chaotic, or random.[2]

Whenever the motion is confined within a finite region of space, an alternative approach consists in fixing a narrow observation window in the coordinate space. Registering only data within the window is a kind of stroboscopic inspection that provides a clustered set of geometric positions, but now the sequence of return times to the window is erratic if the dynamics is irregular. Such a type of observation has already been used in association with some control techniques.[3]

Here we improve the stroboscopic inspection by an adaptive windowing. Precisely, we position the sampling times upon the information provided by the local variation (expansion or contraction) rates, probed with a sensitivity which is readjusted to cope with the long time trends of the dynamics. The stroboscopic time sequence provides not only useful indicators for the chaotic case, but it also permits discrimination between deterministic and stochastic dynamics.

Let us consider a dissipative dynamics $\dot{\mathbf{x}}=\mathbf{f}(\mathbf{x},\mu)$, where $\mathbf{x}$ is a D dimensional vector and μ a set of control parameters, and start by setting μ in order to have a stable periodic orbit of period $\tilde{\tau}$. A $(D-1)$ dimensional Poincaré section intercepts the orbit at a point which repeats after a time $\tilde{\tau}$. Suppose next that, by a change of μ, the orbit is destabilized toward a chaotic attractor.

Rather than modifying the trajectory as in control methods (see later Sec. IV), we aim at recognizing its unperturbed features. For this purpose, based upon the information provided by the local variation rates, we make the next observation interval shorter or longer than $\tilde{\tau}$, in order to minimize **the variation in width** of the window which includes the two points at the extreme of the interval. This depends crucially on the fact that the expansion or contraction in a given direction i cannot be monotonic in the course of time, since the attractor is confined within a finite support and hence the trajectory undergoes frequent twistings.

Precisely, for each coordinate axis i $(i=1, \ldots, D)$, we consider the variation

$$\delta x_i(t_{n+1})=x_i(t_{n+1})-x_i(t_n), \tag{1}$$

where $t_{n+1}-t_n=\tau_n$ is the nth adjustable interval, to be specified. The goal of the adaptive windowing is to keep the separation between two successively observed coordinates as stable as possible, that is, to minimize the variations of δx_i. In order to assign τ_{n+1} we consider the local variation rate

$$\lambda_i(t_{n+1})=\frac{1}{\tau_n}\log\left|\frac{\delta x_i(t_{n+1})}{\delta x_i(t_n)}\right|. \tag{2}$$

Here τ_n is the **minimum of all** $\tau_n^{(i)}$ corresponding to all different i, updated by the rule

$$\tau_{n+1}^{(i)}=\tau_n^{(i)}(1-\tanh(\sigma\lambda_i(t_{n+1}))). \tag{3}$$

The hyperbolic tangent function maps the whole range of $\sigma\lambda_i$ into the interval $(-1,+1)$. The constant σ, strictly positive, is chosen in such a way as to forbid $\tau_{n+1}^{(i)}$ from going to zero. It may be taken as an *a priori* sensitivity. A more sensible strategy would consist in looking at the unbiased dynamical evolution for a while and then taking a σ value smaller than the reciprocal of the maximal λ recorded in that time span. Fixing σ is like fixing the connectivities of a neural network by a preliminary learning session, while adjusting σ upon the information accumulated over previous time steps corresponds to considering σ as a kind of long-term-memory, adding some extra correction to the short-term-memory represented by the sequence of τ_n.[4]

For a fixed σ, the steps of the algorithm are: observation of the data at t_{n+1}; evaluation of $\delta x_i(t_{n+1})$; evaluation of $\lambda_i(t_{n+1})$; updating of $\tau_{n+1}^{(i)}$; selection of $\min_i \tau_{n+1}^{(i)}=\tau_{n+1}$; determination of the new strobing time $t_{n+2}=t_{n+1}+\tau_{n+1}$. This way, we obtain a sequence of observation times starting from given t_0 and $\tilde{\tau}$

$$t_0,\ t_1=t_0+\tilde{\tau},\ t_2=t_1+\tau_1,\ \ldots,t_{n+1}=t_n+\tau_n,\ \ldots \tag{4}$$

corresponding to which the variations of $\delta x_i(t_n)$ can be reduced below a preassigned value. The positions observed at the times t_n are confined within the adaptive window enfolding the trajectory; however the time sequence (4) now includes the chaotic information which was in the original geometric sequence $\mathbf{x}(t)$. Combination of the successive relocation of each τ value with the long time readjustment of the sensitivity σ provides this adaptive strategy with two separate hierarchical levels of control, and hence it is able to cope with singular situations as shown later.

In Ref. 5 we have applied the method to many chaotic situations as the Lorenz model (Lo),[6] the three and four dimensional Roessler model [called respectively Ro3 (Ref. 7) and Ro4 (Ref. 8)] and the Mackey-Glass delay equation (MG).[9]

In fig. 1a x_1 and δx_1 are reported for Ro3. The window δx_1 is confined within a range two orders of magnitude smaller than the variation range of $x_1(t)$. The amount of the reduction factor depends crucially on the chosen σ. Therefore, a trade off between maximal resolution (minimal window variation) and frequency of strobing operations has to be chosen. In fig. 1b the average strobing interval has a length of about 100 integration steps. In order to better illustrate how the algorithm works, fig. 1b offers an expanded time section with x_1 and $\tau^{(1)}$. Figure 1c shows how the strobing interval is selected at any step as the minimum of all $\tau^{(i)}$.

The sequence of strobing intervals contains the relevant information on the dynamics, thus we can characterize chaos as follows. Since in Eq. (3) $|\sigma\lambda_i|\ll 1$, then two successive τ_n must be strongly correlated. Thus, even though the τ_n may be spread over a rather wide support, the return map τ_{n+1} vs τ_n clusters along the diagonal. Any appreciable deviation from the diagonal denotes the presence of uncorrelated noise. This is shown in fig. 2 where we plot the return map of the τ_n for Ro4 and for Ro4 with 1% noise.

The virtue of the adaptive technique consists in an optimized choice among a large number of possibilities offered

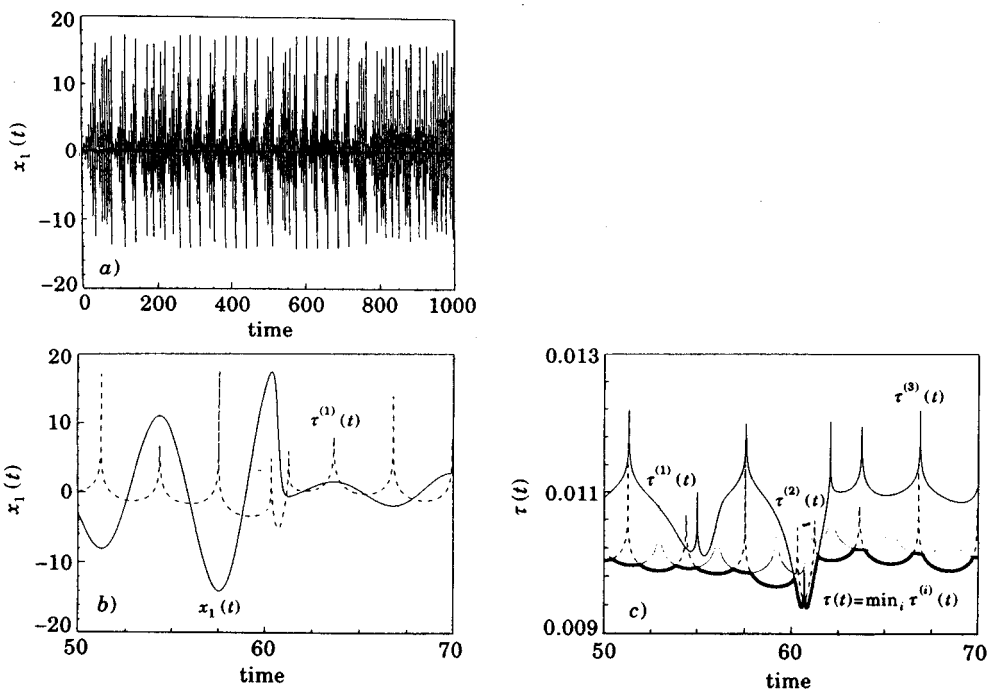

FIG. 1. (From Ref. 5.) Adaptive windowing around the chaotic Ro3 attractor ($a=0.2$, $b=0.2$, $c=9.0$). (a) x_1 and δx_1 (central thick line); $\sigma=0.00015$. (b) Expanded time section of x_1 (solid line) and $\tau^{(1)}$ (dashed line). The vertical scale refers to x_1, while $\tau^{(1)}$ has been translated and expanded to emphasize its correlations with x_1. (c) Plots of $\tau^{(i)}$ $(i=1,2,3)$, showing how the strobing interval is selected as the minimum of the three τ's at any time step.

by the irregular dynamics. In a dissipative chaotic dynamics, the basin of attraction of a given attractor cannot be separated into disjoint sets (ergodic property[10]). As a consequence, for long times the attractor is always reached regardless of the initial condition within the basin. From a heuristic point of view, motion within this basin is equivalent to a dynamics confined within a smooth potential well, whose minima can be reached with little effort. If, however, the potential well becomes too sharp or too flat, the optimal recognition requires a long time readjustment of the sensitivity. This is shown in two cases. Here below we discuss the sharp case, and in Sec. III we will discuss the flat case.

The constant sensitivity recognition becomes critical if applied to a regular orbit, due to the singular invariant distribution of the periodic attractor. In such a case the fixed point τ^* of the τ_{n+1} vs τ_n map displays a structural instability inducing a slow drift. To correct for this, one must recur to the second adaptation level sketched above, that is, change σ upon the information associated with the previous

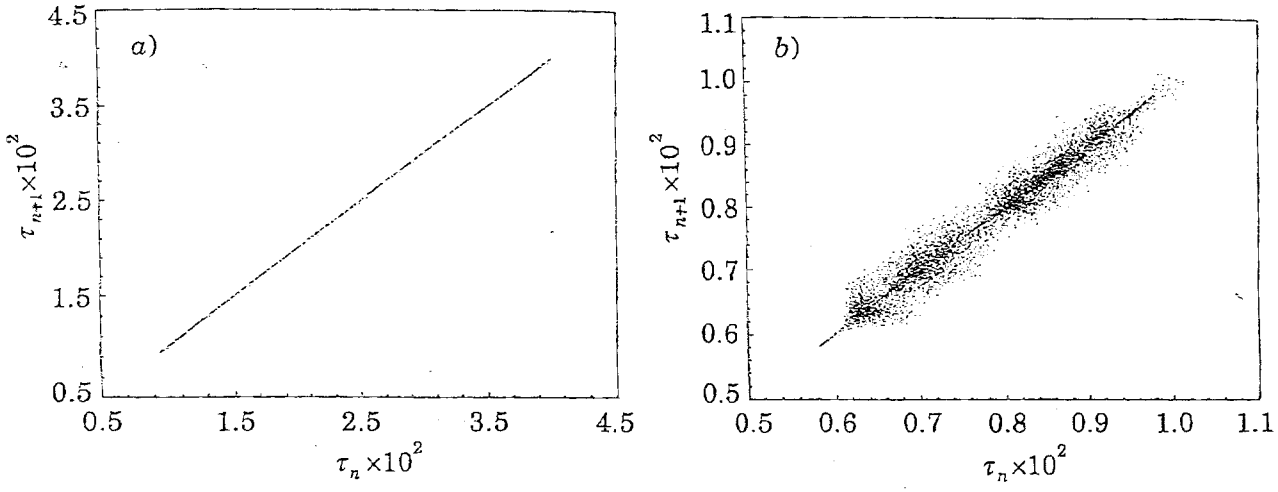

FIG. 2. (From Ref. 5.) Return maps τ_{n+1} vs τ_n for (a) Ro4 and (b) Ro4 with an additional 1% white noise.

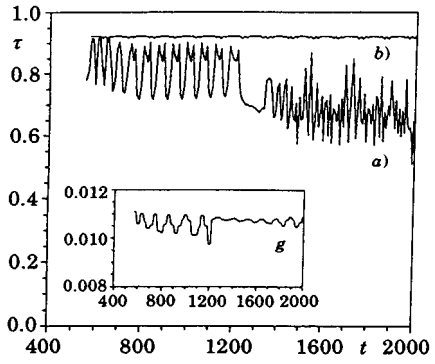

FIG. 3. (From Ref. 5.) Strobing time vs absolute time for a forced oscillator on a periodic orbit. (a) Runaway solution; fixed sensitivity $\sigma=0.05$. (b) Stable solution $\tau=\tau^*\simeq 0.92$; sensitivity adjusted every 30 time steps (inset). $\sigma_0=0.005$.

time steps. This is demonstrated with reference to a forced Duffing oscillator

$$\ddot{x}+0.154\dot{x}-x+4x^3=0.2\cos(1.1t). \tag{5}$$

The selected parameters correspond to a stable periodic orbit. For fixed σ, τ^* runs away. This anomaly disappears by updating σ every 30 observer time steps, with the rule that the new σ is given by

$$\sigma=\sigma_0+\frac{1}{\Sigma|\lambda_i|}. \tag{6}$$

Here the sum is over all i and over all previous 30 time intervals, so that it includes the maximum $|\lambda_i|$ occurring in that time span, and σ_0 is a safety term that provides a minimum sensitivity in case $1/(\Sigma|\lambda_i|)$ gets close to zero. Figure 3 displays the τ sequences for about 400 forcing periods, showing the reliability of our method. In the next section, we will show how Eq. (6) must be written for the general case of a m dimensional subset of a M dimensional dynamics.

To extract a quantitative indicator from the return map τ_{n+1} vs τ_n, we evaluate the average deviation of the observation times away from the diagonal. This should provide an estimate for the maximum Lyapunov exponent Λ_{Max} since, by Eq. (3), the normalized deviation yields the local rate. By direct use of Eq. (2), we propose the following indicator

$$\eta=\frac{1}{M}\sum_{+}\ \sum_{i}\ \lambda_i(t_n), \tag{7}$$

where Σ_+ accounts only for the n_+ cases for which $\mathbf{min}\tau_{n+1}^{(i)}\leqslant\mathbf{min}\tau_n^{(i)}$, Σ_i runs over all m dimensions of the phase space, and $M=Nm$, where $N=n_++n_-$ is the total number of strobing observations ($n_{+(-)}$ is the number of the shrinking (stretching) strobing intervals). The soundness of Eq. (7) is shown by comparing η with Λ_{Max} in the case of Ro3. The positive Lyapunov exponent of Ro3 with $a=b=0.2$, $c=5.7$ and for $N_d=40000$ data turns out to be $\Lambda_{\mathrm{Max}}=0.072\pm0.001$ by the Benettin *et al.* algorithm[11] and $\Lambda_{\mathrm{Max}}=0.075\pm0.005$ by the Sano-Sawada algorithm.[12] Applying our method with a sensitivity $\sigma=0.00038$ to the same system ($\tilde{\tau}=6.3$) and evaluating η for an increasing number of data, η reaches a plateau beyond 6000 data. Its average between 8000 and 12000 data, with three times the standard deviation is $\eta=0.0722\pm0.0003$.

So far we have dealt with an assigned model as Ro3, Ro4 and Lo. A more difficult task is to characterize an empirical time series, in order to discriminate whether it corresponds to a deterministic or stochastic phenomenon. For this purpose we embed our data series in spaces of increasing dimensions. A very stringent test is represented by MG

$$\dot{x}=-0.1x(t)+\frac{0.2x(t-\tau)}{1+x(t-\tau)^{10}}. \tag{8}$$

With $\tau=100$ it corresponds to a ~ 7.5 dimensional chaotic dynamics.

Let us consider the time series for MG, for a pure white noise with r.m.s. fluctuations as MG, and for a random phase time series having the same spectral power as MG (surrogate).[13] For an empirical series of data with no *a priori* information, a discrimination between determinism and noise is provided by the following indicator

$$\beta=\frac{1}{N}\sum_{n}\left|\prod_{i=1}^{m}\lambda_i(t_n)\right|. \tag{9}$$

Its heuristic meaning emerges from the following considerations. Expanding Eq. (2) to first order and referring to the unit time step $\tau_n=1$, we can write $\lambda_i(t_{n+1})=(\delta x_i(t_{n+1})-\delta x_i(t_n))/\delta x_i(t_n)$. We now evaluate the variation over the unit time of the volume $V_n=\Pi_{i=1}^{m}\delta x_i(t_n)$ made by all m measured variations at time t_n. The relative variation rate $r_n=(V_{n+1}-V_n)/V_n$ is given by

$$r_n=\sum_i\ \lambda_i+\sum_{i\neq j}\ \lambda_i\lambda_j+\cdots+\prod_i\ \lambda_i. \tag{10}$$

Summing up over all directions of phase space, we introduce the directional averages

$$\langle\lambda\rangle=\frac{1}{m}\sum_i\ \lambda_i,\ \ \langle\lambda^2\rangle=\frac{2}{m(m-1)}\sum_{i\neq j}\ \lambda_i\lambda_j,\ \ \text{etc.}$$

As we further sum over all n up to N, the twisting along the chaotic trajectory can make all directions statistically equivalent. This occurs whenever the average twisting rate $\langle\Omega\rangle$ introduced in Ref. 14 is larger than the maximum Lyapunov exponent Λ. In such a case, as discussed in that reference, the direction of maximum expansion decorrelates over a time scale less than the dynamical decorrelation time. It is an easy matter to verify that most of the interesting dissipative systems considered in the literature fulfill the condition $\langle\Omega\rangle/\Lambda>1$. Limiting ourselves to this dynamical class, we are entitled to replace $\langle\lambda^k\rangle$ by $\langle\lambda\rangle^k$ for $2\leqslant k\leqslant m$ in $\Sigma_n r_n$. In the case of stochastic noise, since variations over successive time steps are uncorrelated, $\delta x(t_{n+1})-\delta x(t_n)\simeq\delta x(t_n)$ and $\langle\lambda\rangle$ is close to 1, so that $\langle\lambda\rangle^m=O(1)$. Instead for a deterministic dynamics two successive steps are strongly corre-

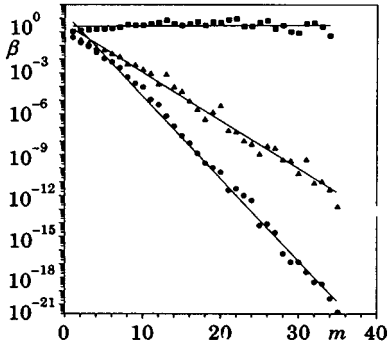

FIG. 4. (From Ref. 5.) β plots vs embedding dimension m. Squares: white noise, triangles: surrogate of MG, circles: MG. For all cases $\sigma=0.0048$. Solid lines are exponential fits $e^{(Am)}$ with $A=0.039$ for white noise, $A=-0.526$ for the surrogate of MG and $A=-0.987$ for MG.

lated, hence $\langle\lambda\rangle<1$, and the last term of Eq. (10), that is $\langle\lambda^m\rangle\sim\langle\lambda\rangle^m=\exp(-m\log(1/\langle\lambda\rangle))$ yields the most sensitive test.

Based on these considerations, we take the sum over the N trajectory points of the last term of Eq. (10) as the β indicator displayed in Eq. (9). In view of what said above, β scales as e^{-m} for a deterministic signal (asides a factor $O(1)$ in the exponent) whereas it scales as e^0 for noise and as $e^{-0.5m}$ for surrogate since one half of the total number of degrees of freedom (phases of the Fourier components) scale like noise and the other half (amplitudes) scale like the deterministic signal.

Figure 4 shows the β plots vs m for MG and its surrogate as well as for white noise. In order to estimate the minimal number $S(m)$ of data necessary for any value m, we start from a very large value S and reduce it until we obtain a deviation $\Delta\beta/\beta\simeq 10\%$. With this definition the number $S(m)$ of data necessary for MG scales as $S(m)=a+bm$, with $a\simeq 10000$ and $b\simeq 3000$.

Comparing our adaptive recognition with statistical methods based upon the assignment of a probability measure in phase-space, as counting the number of neighbors within a given distance from each phase-point[1(a)] or the distribution of distances for closest neighbors,[1(b)] we easily realize that, for S data points, the number of computing operations scales as S in our case and as S^2 in the statistical cases. Furthermore, to assure a good resolution in m embedding dimensions, statistical methods require that $S(m)$ increase exponentially in m, whereas our adaptive strategy is based on variation rates along the coordinate axes and hence our $S(m)$ scales linearly with m as shown above.

III. FILTERING NOISE FROM CHAOS

Adaptive strategy provides a valuable tool for separating noisy contributions from the deterministic part in a chaotic data set. In this section we present a practical implementation, by use of the wavelet transform. The wavelet transform (WT) is a mathematical microscope, whereby a time signal can be decomposed in a representation into both time and frequency. With respect to the Fourier transform (FT), WT has the advantage of localizing the appearance of transient events.

Its application to experimental time series has become widespread[15] in seismic signal analysis,[16] image processing,[17] music,[18] magnetic resonance imaging,[19] image compression,[20] optics,[21] turbulence,[22] neurophysiology,[23] speech discrimination,[24] fractal analysis,[25] DNA sequence analysis,[26] galaxies[27] and asteroids[28] discrimination in observational cosmology.

Here the one dimensional DAUB20 (Ref. 29) version of WT is combined with the adaptive strategy of Sec. II, to provide an efficient filtering process, whereby one can detect and remove additive noise, with no previous knowledge either of the noise correlation properties, or of the dimension of the noiseless data set. The method recognizes and removes frequency by frequency the amount of energy coming from noise, thus reconstructing the deterministic part of the signal.

Given an experimental chaotic signal $x(t)$, for each embedding component i ($i=1, \ldots, m$; m being the selected embedding dimension[30]) one makes use of Eqs. (1)–(3). In this case, however, since the dimension of the process is unknown, the sensitivity of the algorithm must be adjusted. We update σ every L observation time intervals (OTI's), through the rule

$$\sigma=\sigma_0+m\Big/\left(M\sum_{i=1}^{m}\sum_{k=1}^{L}|\lambda_i(t_k)|\right). \tag{11}$$

Here the sum runs over all the actual embedding dimensions ($i=1, \ldots, m$) and over all the previous L OTI's ($k=1, \ldots, L$). $\sigma_0>0$ is a safety term providing a minimum sensitivity in case $1/(\Sigma_{i=1\ldots m}\Sigma_{k=1\ldots L}|\lambda_i(t_k)|)$ gets close to zero.[5] The factor m/M has been introduced to homogeneize the calculation of σ at any embedding dimension. Notice that, when the maximum embedding dimension M is reached, Eq. (11) reduces to the definition introduced for the case of a model problem with preassigned dimensions [see Eq. (6)].

Given an experimental signal $x(t)$ which is the sum of a deterministic and of a noisy part, we act on the coefficients of its WT (obtained with the DAUB20 basis[29]) by eliminating those ones which are smaller than a given threshold θ. The new signal $x'(t)$, generated by inverse WT of the filtered set of coefficients, undergoes the β text. Increasing θ decreases the slope γ of the log $\beta(m)$ plot, down to a saturation value $\overline{\gamma}$ for the corresponding pure deterministic dynamics. Thus, the γ vs θ plot results in a monotonically decreasing function up to $\theta=\overline{\theta}$ where saturation is reached. This way, the minimal threshold $\overline{\theta}$, which extracts from the data as much determinism as possible, is adaptively chosen by the algorithm which drives the filter in wavelet space.

The coupling of WT with our β indicator was extensively treated in Ref. 31.

To show the reliability of this method, we apply it to a set of $\ell=2^{16}$ data extracted from the solution of the delayed Mackey-Glass (MG) equation [Eq. (8)].[9]

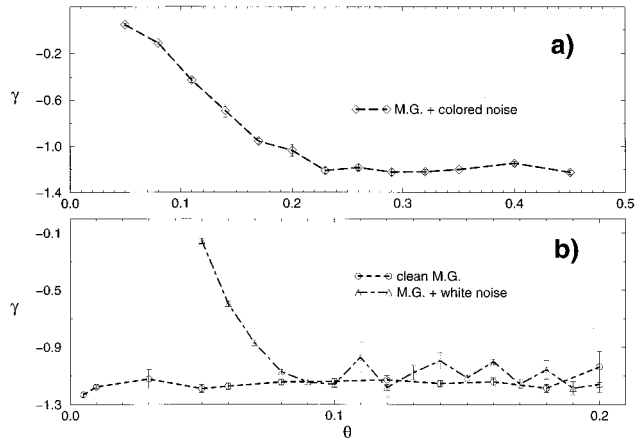

FIG. 5. (From Ref. 30.) γ vs θ plots (see text for definitions). (a) MG plus coloured noise. (b) Pure MG (circles and dashed line) and MG plus white noise (triangles and dot-dashed line). $L=50$, $\sigma_0=5*10^{-6}$, $M=15$.

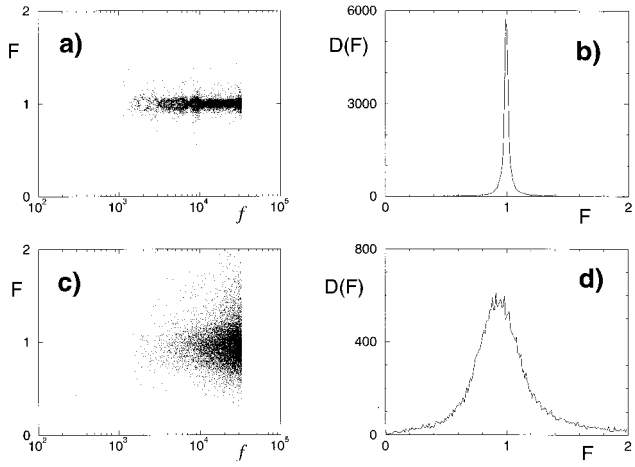

FIG. 7. (From Ref. 30.) Accuracy in the Fourier space reconstruction for MG plus white noise. (a) and (c) report the dimensionless quantity F (see text for definition) vs the frequency channel number f for $\theta=0.1$ and $\theta=0.07$ respectively. (b) and (d) show the corresponding histograms $D(F)$ vs F. Same parameters as in Fig. 5.

For $\tau=100$, MG produces a 7.5 dimensional dynamics.[32] We affect each of the $\mathcal{N}/2$ Fourier components of the above time data with different classes of zero average noise. Precisely, we generate $\mathcal{N}/2$ random Fourier components (amplitudes homogeneously distributed between 0 and 1, phases homogeneously distributed between 0 and 2π), then the inverse FT is normalized in such a way as to produce a noise to signal ratio of 0.02 with respect to MG. This way, we have produced white noise.[33] Limiting the same procedure to a narrower band of Fourier components from the frequency channel f_1 to the frequency channel f_2, we obtain a coloured noise.

Our choice of f_1 and f_2 arises from the following considerations. On one side, a full overlap between the spectra of noise and signal would imply a very difficult filtering task, on the other side, some overlap is needed, otherwise a simple band-cut filter would do the job. In our case, choosing $f_1=2000$ and $f_2=3000$ means working with a non trivial overlap with the power spectrum of MG. In these conditions, any bandpass filter would cause quite big distortions in the reconstruction, insofar as some of the suppressed frequencies would contain relevant information on the deterministic dynamics.

Both white and coloured noise are separately added to MG and the resulting signals have been analyzed with our filter. Figure 5 shows the selection mechanism for the filtering threshold. In both cases, a clear plateau ($\gamma\sim-1.2$) is reached in the corresponding γ vs θ plots, and this plateau corresponds to the γ value for pure MG. The plateau clearly defines the optimal filtering threshold $\overline{\theta}$. Figure 6 gives the reconstructions in the time domain operated by the filter at

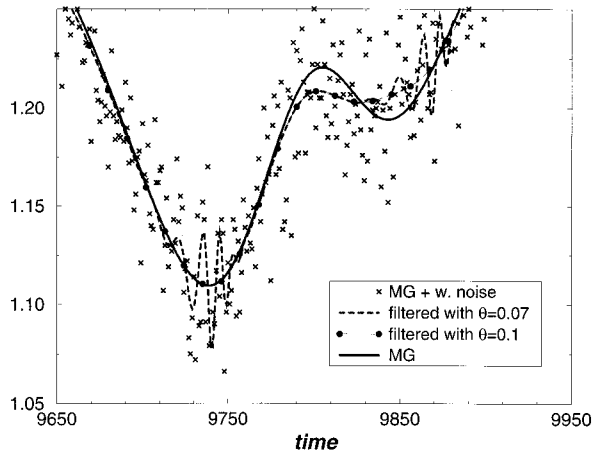

FIG. 6. (From Ref. 30.) Time domain reconstruction of the signal for MG plus white noise. Symbols and lines in the legend. Same parameters as in Fig. 5. Time is in sampling units, the y-axis is labeled in arbitrary units.

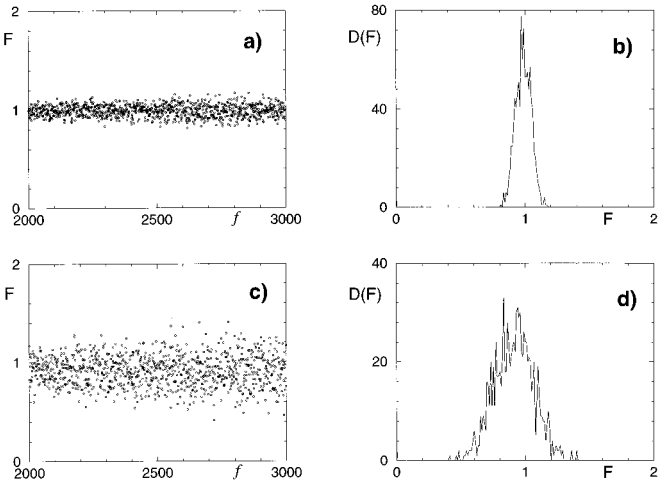

FIG. 8. (From Ref. 30.) Accuracy in the Fourier space reconstruction for MG plus coloured noise (all plots limited to the frequency range covered by the noise). (a) and (c) report the dimensionless quantity F (see text for definition) vs the frequency channel number f for $\theta=0.1$ and $\theta=0.07$ respectively. (b) and (d) show the corresponding histograms $D(F)$ vs F. Same parameters as in Fig. 5.

$\theta = \overline{\theta}$ and $\theta \neq \overline{\theta}$ for the white noise case. The difference in the reconstructions at $\theta = \overline{\theta}$ and $\theta \neq \overline{\theta}$ highlights the effectiveness of the method.

In order to quantify the robustness of the method in analysing and removing the noise from the data, it is worth to refer to the reconstruction of the signal in the frequency domain (Fourier space). A stringent test consists in comparing the amount of energy that the filter eliminates from a given Fourier frequency channel f with the same component of the noise spectrum. We consider the ratio of the amount P_{filtered} of filtered energy to the noise power spectrum P_{noise}. $F(f) = P_{\text{filtered}}(f)/P_{\text{noise}}(f)$ thus measures the accuracy of the filter in recognizing and eliminating the noise component in the channel f. $F(f) = 1$ for any channel f for which the noise has been successfully disentangled from the signal. Figures 7 and 8 report the F vs f plots for MG plus white noise and MG plus coloured noise respectively, calculated at $\theta = \overline{\theta}$ and at $\theta \neq \overline{\theta}$ together with the histograms of the distribution around unity.

It is evident from figs. 7 and 8 that in both cases the best recognition and filtering is obtained for $\theta = \overline{\theta}$.

IV. CONTROL OF CHAOS

Controlling chaos means stabilizing one of the unstable periodic orbits (UPO) (Ref. 34) of a chaotic dynamics by very tiny perturbations which do not affect the main dynamical features.

The different methods for controlling chaos can be classified into two main classes, namely: feedback methods and open loop methods. The first class includes the method proposed by Ott, Grebogi and Yorke (OGY),[35] which consists in readjusting a control parameter each time the trajectory crosses the Poincare' section (PS), the so called occasional proportional feedback (OPF) introduced by Hunt,[3] and the method introduced by Pyragas,[36] based upon a continuous application of a delayed feedback upon one of the system variables.

The second class includes the method of Huebler,[37] which presupposes knowledge of model equations and specifies a goal dynamics to construct control forces, as well as those methods which suppress chaos by means of periodic[38] or stochastic[39] perturbations to the system.

On the other hand, many experimental systems have been studied with the aim of establishing control over chaos, namely: a magneto-elastic ribbon,[40] a thermal convection loop,[41] a yttrium iron garnet oscillator,[42] a diode resonator,[3] an optical multimode chaotic solid-state laser,[43] a Belouzov-Zabotinsky reaction diffusion chemical system,[44] a CO_2 single mode laser with modulation of losses.[45]

Open loop or non-feedback methods are rather limited in their purposes, since they are applicable only to specific dynamical situations already described by a satisfactory model. Furthermore open loop perturbations are not able to select any of the UPO's, but they are limited to some specific dynamical ranges i.e. they are ''goal oriented.'' On the contrary, feedback methods do not presuppose *a priori* knowledge of the model equations, and, after a sufficiently long inspection of the motion features, their control can be applied to any of the UPO's.

All feedback techniques[3,35,36] are affected by some drawback. Precisely, OGY needs a long acquisition section to retrieve the stable and unstable manifolds of the PS saddle point to be controlled. A way out of this limitation was OPF.[3] Its effectiveness has been experimentally demonstrated in Ref. 43. OPF modifies a control parameters of the system by a pulse of fixed duration and amplitude proportional to the separation between a reference line and the extremum of the signal whenever it has entered the selected window. Even though it appears extremely simple, OPF relies on the choice of two quantities (pulse duration and proportionality constant) for which no general criteria have been offered. Furthermore, no application of OPF to chaotic systems with more than one positive Lyapunov exponent has been performed, to our knowledge. Finally, Pyragas[36] controls the UPO's of a system perturbed by a delayed term, hence it is intrinsically based on a delay-differential dynamics which introduces many more dimensions than they were in the original one, including possible spurious UPO's.

Our adaptive technique provides a natural implementation of a feedback control which overcomes the drawbacks sketched above,[46] for the following reasons that we will specify later below: (i) one does not need to retrieve the stability properties of the saddle points, hence the acquisition time is drastically reduced; (ii) one first measures the UPO's periods of the *unperturbed* dynamics, and then applies a control to stabilize a selected UPO; in this operation no spurious UPO's can appear.

For sake of exemplification, let us specialize the generic dissipative chaotic dynamics $\dot{\mathbf{x}} = \mathbf{f}(\mathbf{x}, \mu)$, as the four dimensional Roessler (Ro4) (Ref. 8) model, described by the equations

$$\begin{aligned} &\dot{x}_1 = -x_2 - x_3, \quad \dot{x}_2 = x_1 + 0.25x_2 + x_4, \\ &\dot{x}_3 = 3 + x_1 x_3, \quad \dot{x}_4 = -0.5x_3 + 0.05x_4. \end{aligned} \tag{12}$$

The initial conditions $x_1(0) = -20$, $x_2(0) = x_3(0) = 0$, $x_4(0) = 15$, generates a dynamics with two positive Lyapunov exponents.[8]

The first step of the controlling strategy is to extract the periods of UPO's embedded within the chaotic attractor, by exploiting the sequence of observation time intervals produced as in Sec. II. We then consider the maps τ_{n+k} vs τ_n, $k = 1,2, \ldots$ and plot the r.m.s. η of the point distribution around the diagonal of such maps as a function of k. For a chaotic dynamics, temporal correlations decay over a finite time. Hence, one should expect $\eta(k)$ to be a monotonically increasing function. In fact, the dynamics brings the trajectory to shadow neighborhoods of different UPO's. As it gets close to an UPO of period T_j, the correlation is rebuilt and the distribution of τ includes windows of correlated values appearing as minima of η vs k around $k_j = T_j/\langle\tau\rangle$, $\langle\tau\rangle$ being the average of the τ distribution.

Figure 9 reports the η-k plot for Ro4, from which one can extract the different UPO's periods as the minima of the

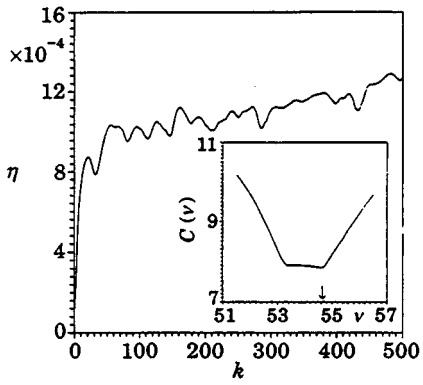

FIG. 9. (From Ref. 45.) $\eta-k$ plot for Ro4. Initial conditions and parameters in the text. $\sigma=0.01$. Inset: cost function $C(\nu)$ for the eighth k minimum of the η curve. $\nu=54.64$ (indicated by the arrow) is the measurement of the period for one of the orbits 8 of Ro4.

η curve. However, since during the observation the time intervals are changing, a rigorous determination of the period can be provided in the following way.

Let $\tau_{\min}$ and $\tau_{\max}$ be respectively the minimum and the maximum τ during the observation. The period T_j of the jth UPO is such that $k_j\tau_{\min}\leqslant T_j\leqslant k_j\tau_{\max}$, where k_j is the jth minimum of the η curve. We introduce a cost function

$$C(\nu)=\sum_{n=1}^{N}|\mathbf{x}(t_n)-\mathbf{x}(t_n-\nu)|, \tag{13}$$

where the sum runs over the N data recorded, and we look for the minimum of $C(\nu)$ with ν ranging from $k_j\tau_{\min}$ to $k_j\tau_{\max}$. Such a minimum measures the period T_j of the jth UPO. The inset of fig. 9 shows the cost function $C(\nu)$ for the eighth minimum of the η plot. $\nu=54.64$ is the period of the 8th UPO of Ro4.

Once periods T_j ($j=1,2,\ldots$) of the UPO's have been extracted, the second step is to achieve stabilization of the desired UPO when the system naturally visits closely phase space neighborhoods of that UPO. At each new observation time $t_{n+1}=t_n+\tau_n$ and for each component i of the dynamics, instead of Eq. (1), we evaluate the differences between actual and desired values:

$$\delta x_i(t_{n+1})=x_i(t_{n+1})-x_i(t_{n+1}-T_j), \tag{14}$$

and the local variation rates λ's now are

$$\lambda_i(t_{n+1})=\frac{1}{\tau_n}\log\left|\frac{x_i(t_{n+1})-x_i(t_{n+1}-T_j)}{x_i(t_n)-x_i(t_n-T_j)}\right|. \tag{15}$$

Eq. (3) and choice of the minimum are kept for the updating process of τ's.

We define $\mathbf{U}(t)$ as the vector with ith component (constant over each adaptive time interval) given by

$$U_i(t_{n+1})=\frac{1}{\tau_{n+1}}(x_i(t_{n+1}-T_j)-x_i(t_{n+1})), \tag{16}$$

and we add such a vector to the evolution equation, which now becomes

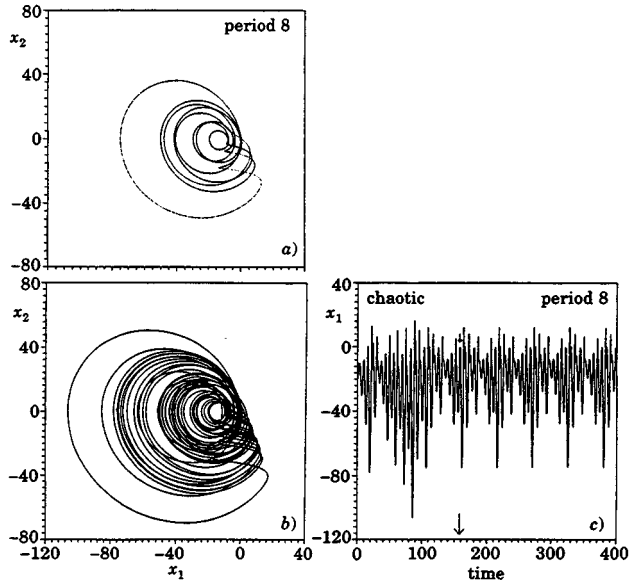

FIG. 10. (From Ref. 45.) (x_1,x_2) projection of the phase space portrait for (a) the controlled period 8 of Ro4, (b) the uncontrolled Ro4. $\sigma=10^{-5}$. (c) Time evolution of the first component x_1 before and after control. Arrow indicates the instance at which control task begins.

$$\frac{d\mathbf{x}}{dt}=\mathbf{f}(x,\mu)+\mathbf{U}(t). \tag{17}$$

The λ's of Eq. (15) measure how the distance between actual and desired trajectory evolves. λ negative means that the true orbit is collapsing into the desired UPO, while λ positive implies that the actual trajectory is diverging away from the UPO and control has to be performed in order to constrain it to shadow the UPO. Contraction or expansion of τ's result in perturbing the dynamics more or less robustly to stabilize the desired UPO, by fixing the weight of the correction, which, once a given T_j has been imposed, is selected by the same adaptive dynamics. The introduced adaptive weighting procedure in Eq. (16) assures the effectiveness of the method (perturbation is larger or smaller whenever it has to be).

In fig. 10 we show the control of period-8 of Ro4. In fig.

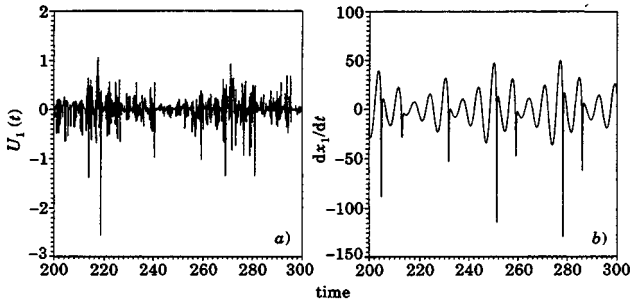

FIG. 11. (From Ref. 45.) (a) Temporal evolution of U_1 (see text for definition) and (b) corresponding evolution of dx_1/dt. Same stipulations for the control task as mentioned in the caption of Fig. 10.

11 we report $U_1(t)$ and $G_1(t)$ for the Ro4 model during control of period-8. It is evident that the former is between two and three orders of magnitude smaller than the latter as expected by the above discussion.

As for time scales, while in Eq. (14) differences δx_i are evaluated with respect to the goal dynamics (thus over the period T_j), in Eq. (15) all λ's are evaluated over the adaptive τ, which has to be larger than the Runge-Kutta integration interval[5] but smaller than the UPO's period (as it is evident from fig. 2 where all k_j's are much above the unity). Thus the method introduces a natural adaptation time scale intermediate between minimum resolution time and time scale of the periodic orbits.

For practical purposes, we can approximate the denominator of Eq. (16) as

$$\tau_{n+1}=\tau_n(1-\mathrm{tgh}(\sigma\lambda_{n+1}))\simeq\langle\tau\rangle(1-\sigma\lambda_{n+1}), \tag{18}$$

where (i) we have replaced τ_n with the ensemble average, and (ii) we have linearized the tgh function. Now, λ_{n+1} of Eq. (15) can also be linearized as

$$\lambda(t)\simeq\frac{1}{\langle\tau\rangle}\frac{\dot{x}(t)-\dot{x}(t-T_j)}{x(t)-x(t-T_j)}, \tag{19}$$

where we have approximated one discretized stroboscopic observation with a continuous inspection. Combining (18) and (19) into Eq. (16) this reduces to

$$U(t)=K_1(x(t-T_j)-x(t))+K_2(\dot{x}(t-T_j)-\dot{x}(t)), \tag{20}$$

where $K_1=1/\langle\tau\rangle$ and $K_2=\sigma/\langle\tau\rangle^2$. This approximation has been suggested by R. Genesio. Its consequences are relevant.

The improvement over Pyragas ($K_2=0$) can be appreciated in a very heuristic way. One single adaptation parameter as K_1 might trap the system within a relative minimum, whereas the presence of two degrees of freedom (K_1 and K_2) allows a global optimization. Furthermore, recently a linearized perturbation technique in terms of a *wash out* filter has been introduced.[47] It consists in dressing the feedback loop with a filter which has zeroes at two frequencies ($\omega=0$ and $\omega=1/T_j$). The filter has the following transfer function ($s=i\omega$ being the frequency domain)

$$W(s)=K_c\frac{s(s^2+\Omega^2)}{(s^2+\xi\Omega s+\Omega^2/4)(s+\nu\Omega)}, \tag{21}$$

where K_c is a gain factor, and $T_j=2\pi/\Omega$ is the period to be stabilized. For appropriate values of ξ and ν see Ref. 47.

Such a wash out filter is of course fully equivalent to Pyragas, in the first approximation. Furthermore the high frequency features introduced by the delay operator $1-e^{-i\omega T_j}$ corresponding to the Pyragas' method are cut off by the polynomial approximation of the filter (21). This filter has been applied to the feedback stabilization of a CO_2 laser.[48] We notice that the linearized version of our adaptive technique reported in Eq. (20) is equivalent to introduce the new filter

$$(K_1+sK_2)W(s). \tag{22}$$

Eq. (22) allows a very convenient hardware implementation of our adaptive control. Since no computational time is prerequired, it is very appropriate for fast chaotic cases, such as laser dynamics.

An extended version of Pyragas technique has been introduced by Bleich and Socolar[49] and later elaborated by Pyragas.[50] It consists in a correction signal which is a sum of contributions at all previous multiples pT_j (p integer) of the chosen period. The above criticism about the high dimensionality of the differential delayed dynamics holds even more. On the other hand, trying to increase the resolution by adding information at previous times is already the virtue of our adaptive technique, but in our case this is done over a set of close-by times, instead of a sparse sampling of the signal at time separations as long as T_j.

V. CHAOS SYNCHRONIZATION

Synchronizing two identical chaotic systems with different initial conditions means linking the trajectory of one system to the same values as the other so that they remain in step with each other, through the transmission of a signal. Pecora and Carrols (PC) (Ref. 51) have shown that this process can be achieved when the sub-Lyapunov exponents for the subsystem to be synchronized are all negative. Since recently the possibility of encoding a message within a chaotic dynamics[52] has been suggested, chaos synchronization can be used to produce message communication between a sender and a receiver.[53] However, several problems arise in order to assure security in the communication. The main one is that the sender must transmit to the receiver at least one of the system variables, and thus a clever spy intercepting the signal can reconstruct the whole dynamics, and decode the message,[54] unless the system is high-dimensional.[55]

Here we show how combining our adaptive scheme with chaos synchronization we can solve the above mentioned drawback which limits the security in the communication, even for a low-dimensional system with a single positive Lyapunov exponent.[56] Suppose to have a message sender (Alice) and a receiver (Bob) in the presence of a spy (James) ready to intercept and decode any communication between them. Alice is made of two identical chaotic systems

$$\dot{\mathbf{x}}_1=\mathbf{f}(\mathbf{x}_1,\mu),\quad \dot{\mathbf{x}}_2=\mathbf{f}(\mathbf{x}_2,\mu),$$

where $\mathbf{x}_1,\mathbf{x}_2$ are two D-dimensional vectors ($D\geqslant 3$), and Bob consists of a third identical system

$$\dot{\mathbf{x}}_3=\mathbf{f}(\mathbf{x}_3,\mu).$$

The three systems start from different initial conditions, thus producing unsynchronized dynamics. In the following the three systems will be represented by the three variable Lorenz system.[6] The vectors $\mathbf{x}_j\equiv(x_j,y_j,z_j)$, $(j=1,2,3)$ obey the equations:

$$\begin{aligned}\dot{x}_j&=10(y_j-x_j),\\ \dot{y}_j&=60x_j-y_j-x_jz_j,\\ \dot{z}_j&=-8/3z_j+x_jy_j.\end{aligned} \tag{23}$$

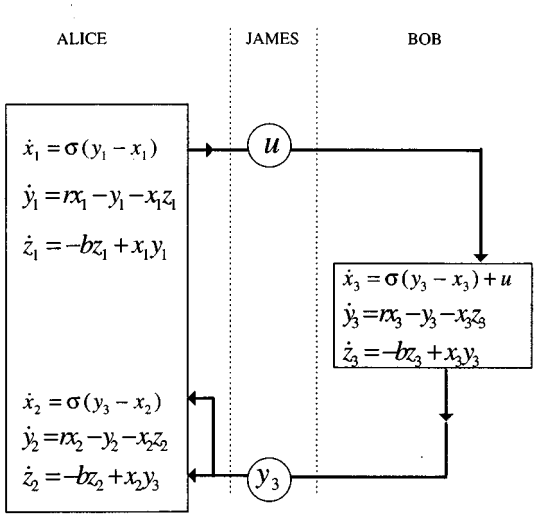

FIG. 12. (From Ref. 55.) The scheme for adaptive synchronization. Bob sends to Alice y_3. Alice sends to Bob $U(t)$. James intercepts both $U(t)$ and y_3.

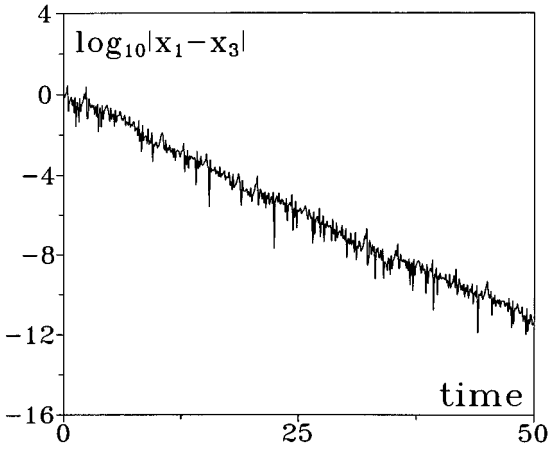

FIG. 13. (From Ref. 55.) Temporal evolution of the quantity $\log_{10}|x_1-x_3|$ measuring the degree of synchronization between Alice and Bob. $\sigma=0.011$, $K=0.1$.

The message Alice must transmit to Bob is encoded in the variable $x_1(t)$. The scheme for the communication is represented in fig. 12. The first step is to synchronize $\mathbf{x}_2$ with $\mathbf{x}_3$. Bob sends to Alice $y_3(t)$ which replaces y_2 into the equations for x_2 and z_2. Synchronization is obtained because the sub-Lyapunov exponents for (x_2,z_2) are both negative.[51] Then Alice knows the actual dynamical state of Bob and can transmit the perturbation $U(t)$ to be applied to the x_3 equation in order to synchronize $\mathbf{x_3}$ to $\mathbf{x}_1$. Alice makes use of Eqs. (1)–(3) with $\delta(t_{n+1})=x_2(t_{n+1})-x_1(t_{n+1})$.

The signal Alice sends to Bob is then

$$U(t)=\frac{K}{\tau_{n+1}}(x_1(t)-x_2(t)), \tag{24}$$

$(K>0)$ which is added to the evolution equation for x_3. Figure 13 reports the temporal behavior of $\Delta x=|x_1-x_3|$ which demonstrates how Alice is synchronized to Bob. Similar results hold also for $|y_1-y_3|$ and $|z_1-z_3|$, thus indicating that $\mathbf{x}_1$ and $\mathbf{x}_3$ are globally synchronized, and any message within x_1 is received and decoded by Bob.

Let us now discuss the problem of security. James intercepts $U(t)$ and $y_3(t)$. No information on x_1 can be retrieved from $U(t)$ since this signal vanishes as soon as Alice and Bob are synchronized, and the weighting factor K/τ_{n+1} is not decided *a priori*, but it is continuously changed, so that no fixed rule is available to James to decode the signal. However, from y_3, James could reconstruct the whole attractor corresponding to $\mathbf{x}_3$, and decode the message once $\mathbf{x}_3$ and $\mathbf{x}_1$ becomes synchronized. To prevent for this, once Alice and Bob have previously agreed on a given accuracy θ in the message, each time such an accuracy has been reached (Alice can test on it), Bob stops sending y_3 for a blank interval T_0. After T_0 Bob starts again sending y_3. If T_0 exceeds the reciprocal of the maximum Lyapunov exponent Λ, the effective signal sent by Bob to Alice results in a collection of uncorrelated subsequences, and no reconstruction of $\mathbf{x}_3$ is possible by James.

This relies crucially on the robustness of our method. In fig. 14 we report the results for $T_0=1$ and $\theta=10^{-5}$ (in our case $\Lambda\simeq 1.41$, so that $T_0>1/\Lambda\simeq 0.71$). The adaptive scheme is able to maintain the stipulated accuracy (fig. 14a) even when the signal sent by Bob to Alice is affected by large holes (fig. 14b) which prevent any external reconstruction of $\mathbf{x}_3(t)$. Figure 14c shows the controlling signal which is still confined within a negligible range $(-10^{-4}-10^{-4})$ with respect to the x_1 dynamics (x_1 variations from -28 to 28).

In conclusion, having solved the problem of secure communication with a low-dimensional system allows an easy hardware implementation as a single integrated element of a communication channel.

VI. TARGETING OF CHAOS

Targeting of chaos means providing small, judiciously chosen perturbations to a chaotic dynamical system to steer the orbit of a given point to a neighborhood of some prespecified point (target) within a specific time. In many practical cases, a small neighborhood of a given attractor point may be visited infrequently, and the unperturbed dynamics may take a long time to approach it, while efficient targeting methods can reduce such a waiting time by orders of magnitude.[57]

The basic algorithm of Ref. 57 consists in finding two successive changes of a control parameter (or one change of two control parameters) to move the image of the starting point onto the stable manifold of the target. The procedure, however, has two main limitations: (i) it is only applicable to invertible mappings and (ii) it needs full *a priori* information on the stable and unstable manifolds of the target points; this latter requirement is a problem when the target is rarely visited by the natural evolution of the system, because the al-

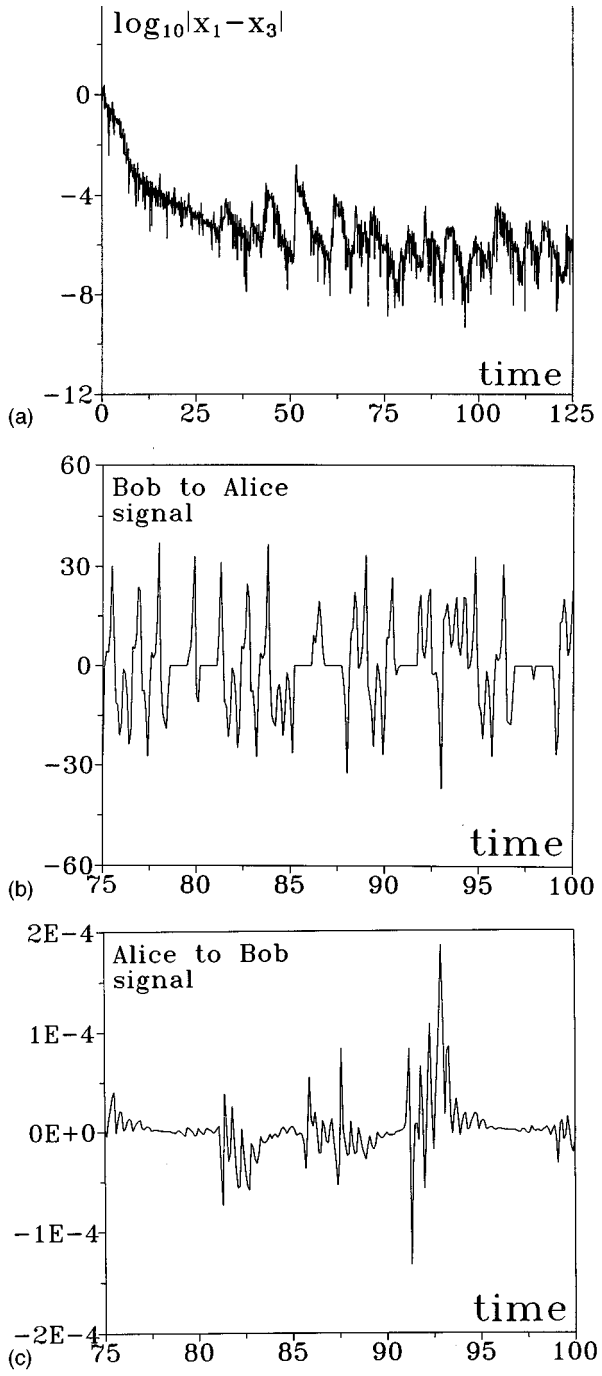

FIG. 14. (From Ref. 55.) (a) Temporal evolution of $\log_{10}|x_1-x_3|$ for $\theta=10^{-5}$ and $T_0=1$. (b) The signal that Bob sends to Alice is affected by large holes, that prevent any possible reconstruction of the message. (c) The controlling signal is kept within a negligible range with respect to the dynamics. Other parameters as in Fig. 13.

gorithm requires a long data acquisition time to obtain points whose orbits visit neighborhoods of the target.

Recently[58] we have presented two adaptive strategies for targeting of chaos that overcome the above difficulties. In particular they do not require apriori information about stable and unstable manifolds of the target point, nor are they restricted to invertible mappings. Finally, they require a single probing of the target, thus drastically reducing the acquisition time.

Let us consider a chaotic process ruled by $\dot{\mathbf{x}}=\mathbf{f}(\mathbf{x},\mu)$, where $\mathbf{x}$ is a D-dimensional vector ($D\geqslant 3$). The targeting procedure consists of two parts: (i) the adaptive algorithm of Sec. II, used in this case to slave the chaotic dynamics $\mathbf{x}(t)$ to a given goal dynamics $\mathbf{g}(t)$, and (ii) the construction of a goal dynamics $\mathbf{g}_T(t)$ compatible with the natural evolution of the system and that brings the trajectory to a small neighborhood of the target within the desired target time starting from a given initial condition $\mathbf{g}_T(0)=\mathbf{g}_0$ (the point $\mathbf{g}_0$ lies on the attractor, and its neighborhood is frequently visited by the unperturbed dynamics).

Reference 58 considered the following cases: (a) the system allows detection and perturbation of all its state variables; and (b) only a single state variable is available for observation.

Let us start with case (a). We use the algorithm of Eqs. (1)–(3) with $\delta_i(t_{n+1})=x_i(t_{n+1})-g_i(t_{n+1})$. The perturbation consists of the vector $\mathbf{U}(t)\equiv(U_1,U_2,\ \ldots\ ,U_D)$ given by

$$U_i(t_{n+1})=\frac{K_i}{\tau_{n+1}}[g_i(t_{n+1})-x_i(t_{n+1})],\quad K_i>0, \tag{25}$$

to be added to evolution equation, which now becomes $\dot{\mathbf{x}}=\mathbf{f}(\mathbf{x},\mu)+\mathbf{U}(t)$. We now need to extract a goal dynamics $\mathbf{g}_T(t)$ from a preliminary observation of the unperturbed behavior of the system. We consider the three-dimensional Rössler system[7]

$$\begin{aligned}\dot{x}&=-z-y,\\ \dot{y}&=x+0.2y,\\ \dot{z}&=0.2+z(x-5.7).\end{aligned} \tag{26}$$

We first construct a partition of the phase space in parallelograms of sides $\epsilon\equiv(\epsilon_1,\epsilon_2,\epsilon_3)$. We define

$$I(x_0,y_0,z_0,\epsilon)=\{(x,y,z):x_0<x<x_0+\epsilon_1,y_0<y<y_0+\epsilon_2,\ \text{and}\ z_0<z<z_0+\epsilon_3\}.$$

The initial condition $x(0)=y(0)=1$, $z(0)=4$ gives rise to a chaotic set, a portion of which is within the parallelogram $I_T(4.655146,-6.691886,0.013528,\epsilon)$, where $\epsilon\equiv(0.205382, 0.186303,0.228361)$. ($t=t_T=9743.658203$ is the time at which the unperturbed trajectory first enters I_T). Let $P(I_T)$ denote a preimage of I_T. We record the portions of the observed trajectories that lie in I_T and $P(I_T)$, and determine successive preimages of $P(I_T)$, which, in most cases, have been visited previously by the portions of the observed trajectories. Going backward in time, we can select from the observations a path that starts from the most frequently visited parallelogram I_F and leads to the box I_T containing the target. The web of paths is illustrated schematically in fig. 15. This construction requires only a single probing of the target.

The goal dynamics is an observed path from I_F to I_T. Since the natural measure of I_F is large (that is, it is fre-

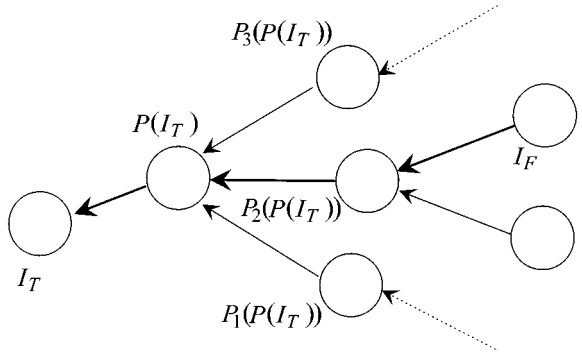

FIG. 15. (From Ref. 57.) Procedure for the construction of the goal dynamics. Each bubble represents the neighborhood of a point in the phase space. I_T: target; $P(I_T)$: unique preimage of the target; $P_j(P(I_T)), j=1,2,3$: multiple preimages of $P(I_T)$; I_F: most frequently visited parallelogram. The selected path is shown as a thick line.

quently visited by the unperturbed dynamics), the target can be reached quickly regardless of the initial conditions.

Figure 16a reports the results of this targeting procedure. In the trials reported here, I_F is reached by the unperturbed dynamics for the first time when $t=30.9$ seconds, and then I_T is reached by the perturbed dynamics only 1.6 seconds later. Thus, the total time required to reach the I_T is 32.5 seconds, compared to 9743 seconds for the unperturbed dynamics to enter the same neighborhood, for a total speedup of two orders of magnitude. Figure 16b illustrates the mechanism that leads the system to the target: the path that is followed by the targeting algorithm moves from high probability sections of the attractor toward lower probability sections of the same attractor, eventually reaching the desired target.

This procedure, however, requires all state variables to be accessible for measurement and perturbation. Thus it cannot be applied in experimental situations, where often only a single state variable of the system is accessible. We now show how to reformulate the adaptive targeting strategy by restricting our measurements only to the x variable of the Rössler system and applying the feedback perturbation only on the first of Eqs. (26).

The control procedure defined by Eqs. (26) is effective in low- and high-dimensional cases even if the perturbations are restricted to a single state variable. Thus we can restrict attention to the case $i=1$.

The problem is to retrieve a suitable scalar goal dynamics $g(t)$ from the observations that is compatible with the unperturbed evolution of the system and comes at least once within a suitable neighborhood of the target. We will use the time delay embedding method,[30] which allows us to reconstruct the attractor from a time series of measurements of a single variable, say $x(t)$, from Eqs. (26). By selecting a suitable delay time $\tilde{\tau}$, we consider the D-dimensional embedding space containing the vectors $\mathbf{x}(t)\equiv(x(t),x(t-\tilde{\tau}),\ldots,x(t-(D-1)\tilde{\tau}))$ ($D=3$ in our case). The reconstructed attractor retains the basic metric properties of the original; that

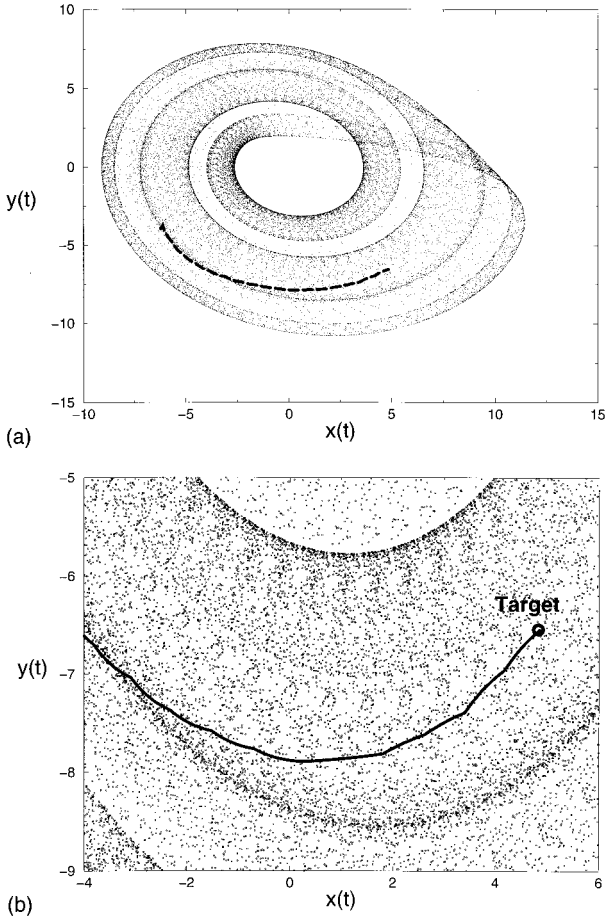

FIG. 16. (From Ref. 57.) (a) An (x,y) projection of the unperturbed Ro3 (dots) and of the path followed by the perturbed Ro3 to reach the target (thick dashed line). (b) Enlargement of (a): the path (solid line) moves from high probability sections of the attractor toward lower probability sections, until reaching I_T (indicated as ''Target'' in the figure). $\sigma=10^{-5}$, $K_1=K_2=K_3=0.01$.

is, points that are neighbors in the original phase space with respect to a given metric M_R remain neighbors in the embedding space with respect to some new metric M_E.[59]

With $\tilde{\tau}=5.71157$, the target point in the original phase space, as discussed in the first example, corresponds to the point $\mathbf{x}_T=(x_T(t_T),x_T(t_T-\tilde{\tau}),x_T(t_T-2\tilde{\tau}))=(4.727415, 4.295067,4.929038)$, where t_T is the time at which the unperturbed trajectory first enters the neighborhood of the target. The idea is to retrieve a scalar goal dynamics $g(t)$ such that $g(t_0)=x_T(t_T-2\tilde{\tau})$, $g(t_0+\tilde{\tau})=x_T(t_T-\tilde{\tau})$, and $g(t_0+2\tilde{\tau})=x_T(t_T)$. Here t_0 is the instant at which the unperturbed dynamics $x(t)$ first satisfies the relations $x_T(t_T-2\tilde{\tau})-\epsilon_1/2<x(t)<x_T(t_T-2\tilde{\tau})+\epsilon_1/2$, where $\epsilon_1=0.205382$. These requirements assure that the perturbations move a trajectory to the target within a target time $t_0+2\tilde{\tau}$, starting from any initial condition.

The simplest choice of g is the recorded unperturbed evolution of x from $t_T-2\tilde{\tau}$ to t_T. It is possible that such a choice of g is not optimal. Indeed, since our observations and perturbations are limited to a one-dimensional subspace

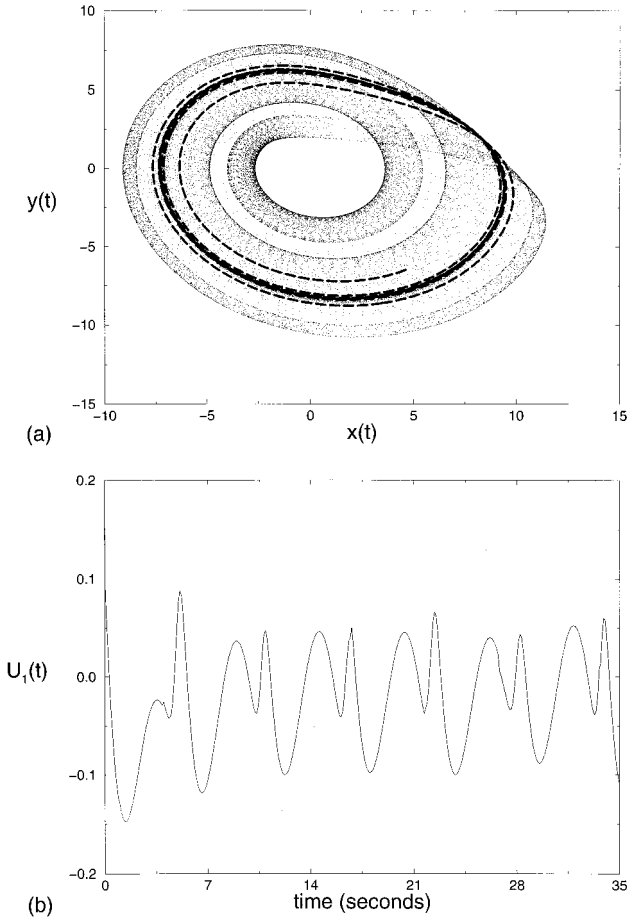

FIG. 17. (From Ref. 57.) (a) An (x,y) projection of the unperturbed Ro3 (dots) and path followed by the perturbed dynamics to reach the target (thick dashed line). In this case the perturbation acts only on the x variable. The path is inside the chaotic attractor; thus it is compatible with the natural evolution of the system, and it goes from higher to lower probability regions. (b) Temporal evolution of the perturbation during the targeting process. The range spanned by U_1 is less than 1% of the range spanned by the x dynamics. Initial conditions and parameters as in the caption of Fig. 16, $K_1=0.02$.

of the original phase space, there is no certainty that at $t=t_0$ (the instant at which the variable x first enters the ϵ_1 interval of $x_T(t_T-2\tilde{\tau})$), the other unobserved variables are within a sufficiently small distance from their values at $t_T-2\tilde{\tau}$. The process could result in an unacceptably large initial perturbation, so that another choice of g would be necessary. In our case, it is sufficient to choose $g(t)$ as the unperturbed dynamics from $t_T-N\tilde{\tau}$ to t_T $(N>2)$ to guarantee fast convergence to the target even for small perturbations. While the integer N should be selected as small as possible to minimize the waiting time, larger values of N improve the robustness of the method. Figure 17a reports the new phase space results for $N=6$. The system has been left unperturbed from $t=0$ (the same initial conditions as before) until $t=t_0=12.9$. Here t_0 is the instant at which the unperturbed dynamics first enters the ϵ_1 interval containing $x(t_T-6\tilde{\tau})$. The adaptive scalar perturbation has assured a convergence to the target within a target time of $t_0+6\tilde{\tau}$, which again is more than two orders of magnitude smaller than t_T.

The reconstruction in the real space represents a stringent test, since it demonstrates the accuracy and robustness of our method in targeting the desired I_T, even with the simplest choice of g. Figure 17b shows the range of fluctuations of the perturbation, and fig. 17a shows the range spanned by the unperturbed x dynamics. These results illustrate the smallness of the perturbation required by the adaptive method.

VII. CONCLUSIONS

Adaptive recognition is a rather limited endeavor as compared to global information acquisition. It consists in a hierarchical classification of cognitive goals, picking up a limited set and overlooking all the other ones. Since global information would require an infinite acquisition time and infinite resolution, any wise cognitive task is necessarily adaptive, as illustrated by the history of life in this planet and as stated by the scientific ''manifesto,'' the so called Occam razor (do not increase the number of explanations beyond necessity).

Applying these general considerations to a chaotic dynamics, the standard reconstruction of the D-dimensional phase space geometry provides in general an excess of information as compared to our limited ambitions. In particular, when dealing with time aspects of a dissipative chaotic dynamics such as the value of the maximum Lyapunov exponent or the periods of the UPO's contained in the attractor, or trying to control or synchronize this dynamics, it seems sufficient to rely on a one dimensional string of data, i.e. the ordered sequence of those observation times which minimize the difference in the geometric distances between pairs of adjacent points.

Adaptation stems from a local variation tactics combined with a long time strategy consisting in a slow readjustment of the sensitivity. For a well defined goal (control or synchronization) the adaptive procedure can be implemented into a device, highly useful in technical applications.

The very smooth increase of the computational time with the complexity of the system (number of dimensions and duration of the observation, that is, number of data points) suggests that an adaptive strategy should be useful in recognizing or controlling high-dimensional systems, as delayed dynamics or extended patterns.[60]

ACKNOWLEDGMENTS

The authors acknowledge G. Basti, A. Farini, R. Genesio, A. Giaquinta, E.J. Kostelich, and A.L. Perrone for active collaborations in parts of this work, and for helpful general discussions.

[1] (a) P. Grassberger and I. Procaccia, Phys. Rev. Lett. **50**, 346 (1983); (b) R. Badii and A. Politi, *ibid.* **52**, 1661 (1984).
[2] H. D. I. Abarbanel, R. Brown, J. J. Sidorowich, and L. Sh. Tsimring, Rev. Mod. Phys. **65**, 1331 (1993); A. S. Weigend and N. A. Gershenfeld, *Times Series Prediction: Forecasting the Future and Understanding the Past* (Addison–Wesley, Reading, 1993).

[3] E. R. Hunt, Phys. Rev. Lett. **67**, 1953 (1991).
[4] S. Grossberg, Neural Networks **1**, 17 (1988).
[5] F. T. Arecchi, G. Basti, S. Boccaletti, and A. L. Perrone, Europhys. Lett. **26**, 327 (1994).
[6] E. N. Lorenz, J. Atmos. Sci. **20**, 130 (1963).
[7] O. E. Roessler, Phys. Lett. A **57**, 397 (1976).
[8] O. E. Roessler, Phys. Lett. A **71**, 155 (1979).
[9] M. C. Mackey and L. Glass, Science **197**, 287 (1977).
[10] J. P. Eckmann and D. Ruelle, Rev. Mod. Phys. **57**, 617 (1985).
[11] G. Benettin, L. Galgani, A. Giorgilli, and J.-M. Strelcyn, Meccanica **15**, 9 (1980).
[12] M. Sano and Y. Sawada, Phys. Rev. Lett. **55**, 1082 (1985).
[13] J. Theiler *et al.*, in *Nonlinear Modeling and Forecasting*, edited by M. Casdagli and S. Eubank (Addison–Wesley, Reading, 1992).
[14] A. Farini, S. Boccaletti, and F. T. Arecchi, Phys. Rev. E **53**, 4447 (1996).
[15] I. Daubechies, IEEE Trans. Inf. Theory **36**, 961 (1990).
[16] P. Goupillaud, A. Grossmann, and J. Morlet, Geoexploration **23**, 85 (1984).
[17] S. G. Mallat, IEEE Trans. Acoust. Speech Signal Process. **37**, 2091 (1989).
[18] R. Kronland-Martinet, J. Morlet, and A. Grossmann, Int. J. Pat. Recog. Artif. Intell. **1**, 97 (1987).
[19] J. B. Weaver, Y. Xu, D. M. Healy, and J. R. Driscoll, Magn. Reson. Med. **24**, 275 (1992).
[20] R. A. De Vore, B. Jawerth, and B. J. Lucier, IEEE Trans. Inf. Theory **38**, 719 (1992).
[21] B. Pouligny, G. Gabriel, J. F. Muzy, A. Arneodo, and F. Argoul, J. Appl. Crystallogr. **24**, 526 (1991).
[22] F. Argoul, A. Arneodo, G. Grasseau, Y. Gagne, E. J. Hopfinger, and U. Frisch, Nature (London) **338**, 51 (1989).
[23] A. W. Przybyszewski, J. Neurosci. Methods **38**, 247 (1991).
[24] S. Kadambe and G. F. Boudreaux-Bartels, IEEE Trans. Inf. Theory **38**, 917 (1992).
[25] A. Arneodo, G. Grasseau, and M. Holdschneider, Phys. Rev. Lett. **61**, 2281 (1988).
[26] A. Arneodo, E. Bacry, P. V. Graves, and J. F. Muzy, Phys. Rev. Lett. **74**, 3293 (1995).
[27] E. Slezak, A. Bijaoui, and G. Mars, Astron. Astrophys. **227**, 301 (1990).
[28] Ph. Bendjoya, E. Slezak, and CI. Froeschle, Astron. Astrophys. **251**, 312 (1991).
[29] I. Daubechies, *Wavelets* (S.I.A.M., Philadelphia, 1992).
[30] F. Takens, *Detecting Strange Attractors in Turbulence*, Lecture Notes in Math (Springer, Berlin, 1981), Vol. 898.
[31] S. Boccaletti, A. Giaquinta, and F. T. Arecchi, Phys. Rev. E **55**, 5393 (1997).
[32] J. D. Farmer, Physica D **4**, 366 (1982).
[33] S. O. Rice, Bell Syst. Technol. J. **24**, 46 (1945).
[34] D. Auerbach, P. Cvitanovic, J.-P. Eckmann, G. Gunaratne, and I. Procaccia, Phys. Rev. Lett. **58**, 2387 (1987).
[35] E. Ott, C. Grebogi, and J. A. Yorke, Phys. Rev. Lett. **64**, 1196 (1990).
[36] K. Pyragas, Phys. Lett. A **170**, 421 (1992).
[37] B. B. Plapp and A. W. Huebler, Phys. Rev. Lett. **65**, 2302 (1990); E. A. Jackson and A. W. Huebler, Physica D **44**, 407 (1990).
[38] R. Lima and M. Pettini, Phys. Rev. A **41**, 726 (1990).
[39] Y. Braiman and I. Goldhirsch, Phys. Rev. Lett. **66**, 2545 (1991).
[40] W. L. Ditto, S. N. Rauseo, and M. L. Spano, Phys. Rev. Lett. **65**, 3211 (1990).
[41] J. Singer, Y.-Z. Wang, and H. H. Bau, Phys. Rev. Lett. **66**, 1123 (1991).
[42] A. Azevedo and S. M. Rezende, Phys. Rev. Lett. **66**, 1342 (1991).
[43] R. Roy, T. W. Murphy, Jr., T. D. Maier, Z. Gills, and E. R. Hunt, Phys. Rev. Lett. **68**, 1259 (1992).
[44] (a) B. Peng, V. Petrov, and K. Showalter, J. Phys. Chem. **95**, 4957 (1991); (b) V. Petrov, V. Gaspar, J. Masere, and K. Showalter, Nature (London) **361**, 240 (1993).
[45] R. Meucci, W. Gadomski, M. Ciofini, and F. T. Arecchi, Phys. Rev. E **49**, R2528 (1994).
[46] S. Boccaletti and F. T. Arecchi, Europhys. Lett. **31**, 127 (1995).
[47] M. Basso, R. Genesio, and A. Tesi, Syst. Contr. Lett. (to be published).
[48] R. Meucci, M. Ciofini, and R. Abbate, Phys. Rev. E **53**, R5537 (1996).
[49] D. J. Gauthier, D. K. Sukow, H. M. Concannon, and J. E. S. Socolar, Phys. Rev. E **50**, 2343 (1994); J. E. S. Socolar, D. K. Sukow, and D. J. Gauthier, *ibid.* **50**, 3245 (1994).
[50] K. Pyragas, Phys. Lett. A **206**, 323 (1995).
[51] L. M. Pecora and T. L. Carrols, Phys. Rev. Lett. **64**, 821 (1990).
[52] S. Hayes, C. Grebogi, E. Ott, and A. Mark, Phys. Rev. Lett. **73**, 1781 (1994).
[53] K. M. Cuomo and A. V. Oppenheim, Phys. Rev. Lett. **71**, 65 (1993).
[54] G. Perez and H. A. Cerdeira, Phys. Rev. Lett. **74**, 1970 (1995).
[55] J. H. Peng, E. J. Ding, M. Ding, and W. Yang, Phys. Rev. Lett. **76**, 904 (1996).
[56] S. Boccaletti, A. Farini, and F. T. Arecchi, Phys. Rev. E **55**, 4979 (1997).
[57] T. Shinbrot *et al.*, Phys. Rev. Lett. **65**, 3215 (1990); T. Shinbrot *et al.*, Phys. Rev. A **45**, 4165 (1992); T. Shinbrot *et al.*, Phys. Rev. Lett. **68**, 2863 (1992); T. Shinbrot *et al.*, Phys. Lett. A **169**, 349 (1992); E. J. Kostelich *et al.*, Phys. Rev. E **47**, 305 (1993).
[58] S. Boccaletti, A. Farini, E. J. Kostelich, and F. T. Arecchi, Phys. Rev. E **55**, R4845 (1997).
[59] In most cases, and also in ours, M_R and M_E both coincide with the metric defining the Euclidean distance between points.
[60] We have already preliminary evidence that the adaptive control stabilizes a chaotic delayed dynamics in a regime where defects and spacelike structures are present. The corresponding report is in preparation.